Calculations of the superconducting critical temperature with vertex corrections

Vladimir N. Kostur* and Božidar Mitrović
Department of Physics, Brock University, St. Catharines, Ontario, Canada L2S 3A1
(Received 6 July 1994)

The calculations of the superconducting transition temperature, including the lowest-order vertex corrections, are carried out for three models: the BCS-type instantaneous interaction, a retarded isotropic interaction described by the Eliashberg spectral function $\alpha^2F(\Omega)$ and a spin-fluctuation interaction with four δ-function peaks in the corners of a square Brillouin zone. In the isotropic case the effect of higher-order self-energy diagrams is to suppress the critical temperature calculated within the mean-field approximation when the characteristic energy of the boson responsible for the pairing is not small compared to the Fermi energy. In the case of the model with sharp peaks in the momentum space the vertex correction can lead to an *increase* of T_c.

I. INTRODUCTION

In spite of the fact that the mechanism of high-temperature superconductivity remains unclear, there are several questions regarding the calculations of T_c that can be addressed, regardless of the symmetry of the order parameter. Firstly, how large is a typical energy of the bosons that mediate pairing compared to the T_c. Secondly, how are the other energy scales, such as the Fermi energy E_F, the bandwidth and the coupling constants, related to the T_c. Thirdly, how does the geometry of the electronic spectra (and/or the anisotropy of the electron-boson interaction) affect the relation between the T_c and the energy scale of the pairing bosons. In the conventional electron-phonon superconductors the main energy scales satisfy the inequalities $T_c < \omega_D \ll E_F$, where ω_D is a typical phonon energy. The BCS theory, which is quantitatively accurate when $T_c \ll \omega_D$, gives $T_c \simeq 1.14\omega_D e^{-1/\lambda} + O(\lambda\omega_D/E_F)$,[1] where λ is the coupling constant, and therefore E_F drops out of the problem with a high accuracy. However, if ω_D/E_F is not small, as has been suggested for fullerenes,[2] the question is what is precisely the sign and the magnitude of the correction to the BCS formula for T_c. The same problems remain in the strong-coupling regime $T_c/\omega_D \simeq 10\%$, in which case the Eliashberg equations[3,4] predict the superconducting transition temperature with the accuracy $O(\omega_D/E_F)$.

For the nonphononic mechanism of superconductivity in electron gas, a detailed numerical study by Rietschel and Sham,[5] who included the full momentum and frequency dependence in the Eliashberg-type equations, indicated that the vertex corrections must have an important effect on T_c. Subsequent calculations by Grabowski and Sham[6] indeed found that T_c decreases drastically when the vertex corrections are included in the calculations. On the other hand, the effect of vertex corrections at a Van Hove singularity leads to modest changes of T_c in a k-averaging approximation for the Green's functions.[7]

In recent calculations of the T_c for antiferromagnetic spin-fluctuation mediated pairing in copper-oxides,[8–10] Eliashberg-type equations, which take into account the momentum dependence of the spin-fluctuation spectral density and of the electronic dispersion over the entire Brillouin zone, were used. These calculations showed that taking into account the full momentum dependence results in a T_c, which is substantially different from the one obtained by keeping all electronic momenta near the Fermi surface.[8,11] The full self-consistent calculations,[12,13] which take into account the effect of pairing correlations on spin-susceptibility calculated in the random-phase approximation (RPA), show that the pairing is strongly affected below T_c. The question remains,[9] how important are the vertex corrections in the spin-fluctuation theories, in spite of the fact that the spectral weight for the spin-susceptibility used in Refs. 8–10 peaks at an energy that is much smaller than the bandwidth (see Ref. 9 and the references therein). Since the spectral function has a nonzero weight at energies that are not small compared to the bandwidth, the sign and the magnitude of the contribution to the T_c arising from the vertex corrections has to be examined quantitatively. Recent quantum Monte Carlo simulations for the two-dimensional Hubbard model[14] indicate that the single spin-fluctuation exchange underestimates the effective particle-particle interaction, and that high-order vertex corrections are required.

In the present paper we examine the effect of vertex corrections for several models. In Sec. II the effect of higher-order diagrams on the T_c equation is studied for the BCS-type interaction. It is found that T_c decreases with increasing $\lambda\omega_D/E_F$ and above some critical value of this parameter the solution of the T_c equation does not exist. In Sec. III the numerical calculations of T_c using the strong-coupling equations with the lowest-order vertex correction are carried out. In the isotropic case the T_c decreases with increasing value of the ratio between the characteristic boson energy and E_F, as in the BCS case. However, for a highly anisotropic model of spin-fluctuation-induced pairing, which is analogous to the models used previously for copper oxides, there is a possibility of the enhancement of T_c by vertex corrections in a certain range of values for the chemical potential μ. The last section gives a summary and conclusions.

II. BCS-INSTANTANEOUS INTERACTION AND T_c-EQUATION

We consider first the Hamiltonian

$$H = \sum_{\mathbf{p}\sigma} \epsilon_{\mathbf{p}} c^{\dagger}_{\mathbf{p}\sigma} c_{\mathbf{p}\sigma} + \sum_{\mathbf{p}_1\sigma,\mathbf{p}_2\sigma',\mathbf{p}_3\sigma',\mathbf{p}_4\sigma}^{\mathbf{p}_1+\mathbf{p}_2=\mathbf{p}_3+\mathbf{p}_4} V_{\mathbf{p}_1\mathbf{p}_2,\mathbf{p}_3\mathbf{p}_4} c^{\dagger}_{\mathbf{p}_1\sigma} c^{\dagger}_{\mathbf{p}_2\sigma'} c_{\mathbf{p}_3\sigma'} c_{\mathbf{p}_4\sigma} \quad (1)$$

with the BCS-type interaction[1]

$$V_{\mathbf{p}_1\mathbf{p}_2,\mathbf{p}_3\mathbf{p}_4} = -V \prod_{\alpha=1}^{4} \theta(\omega_c - |\epsilon_{\mathbf{p}_\alpha}|). \quad (2)$$

In Eq. (2) V is the interaction constant, θ is the step function, ω_c is the half width of the energy shell around the Fermi surface in which the interaction is nonzero, and $\epsilon_{\mathbf{p}}$ is the electron energy. The diagrams with one and two interaction lines in the particle-particle channel for a general two-body (or a boson mediated) interaction are shown in Fig. 1. One can easily obtain from these diagrams the diagrams for the irreducible pairing self-energy[1] *near* T_c by joining together the two incoming lines, as indicated by a dashed line in Fig. 1, and by interpreting the resulting line as the anomalous Gor'kov's Green's function. Clearly, the pairing self-energy diagram generated in this way from the one in Fig. 1(b) is not irreducible and must be left out. The diagrams in Figs. 1(c) and 1(d) involve interaction between particles with parallel spins and are not present for the interaction given by Eq. (2). It is clear that this method could be generalized to include the corrections to the irreducible pairing self-energy near T_c from diagrams with more than two interaction lines, such as the crossed diagram in Fig. 1(e). Using the standard Gor'kov's form for the anomalous Green's function (dashed line in Fig. 1) at T_c

$$F(\epsilon_p, i\omega_n) = \frac{\phi_p(i\omega_n)}{\omega_n^2 + \epsilon_p^2}, \quad (3)$$

where ϕ_p is the pairing self-energy and $i\omega_n = i\pi T(2n-1)$ is a fermion Matsubara frequency, one obtains in this way the equation for ϕ_p near T_c which includes the effect of vertex corrections

$$\phi_p(i\omega_n) = -T \sum_{n'} \sum_{\mathbf{p}'} \left[V_{p,p'}(0) + \delta V^{n,n'}_{p,p'} \right] \frac{\phi_{p'}(i\omega_{n'})}{\omega_{n'}^2 + \epsilon_{p'}^2}. \quad (4)$$

Here

$$V_{p,p'}(0) = -V\theta(\omega_c - |\epsilon_p|)\theta(\omega_c - |\epsilon_{p'}|), \quad (5)$$

and the correction term $\delta V^{n,n'}_{p,p'}$ is due to diagrams with two and more crossed interaction lines. As usual, one can introduce the order parameter

$$\Delta_p = -T \sum_{n'} \sum_{\mathbf{p}'} V_{p,p'}(0) \frac{\phi_{p'}(i\omega_{n'})}{\omega_{n'}^2 + \epsilon_{p'}^2}, \quad (6)$$

which does not depend on Matsubara frequency $i\omega_n$. Equations (4) and (6) imply the following equation for Δ_p:

$$\Delta_p = -T \sum_{n'} \sum_{\mathbf{p}'} \frac{V_{p,p'}(0)}{\omega_{n'}^2 + \epsilon_{p'}^2} \Delta_{p'} + T^2 \sum_{n',n''} \sum_{\mathbf{p}',\mathbf{p}''} \frac{V_{p,p'}(0)\delta V^{n',n''}_{p',p''}}{(\omega_{n'}^2 + \epsilon_{p'}^2)(\omega_{n''}^2 + \epsilon_{p''}^2)} \Delta_{p''} + O(|\delta V^{n,n'}_{p,p'}|^2). \quad (7)$$

The usual BCS equation for T_c is obtained by retaining only the first term in Eq. (7). In the following we assume that $\lambda = N(0)V$, where N(0) is the electronic density of states at the Fermi level, is less than 1 so that $\delta V^{n,n'}_{p,p'}$ is small and could be approximated by the contribution from two crossed interaction lines.[15] Then the term $O(|\delta V^{n,n'}_{p,p'}|^2)$ in Eq. (7) could be ignored, and using the bare Green's functions for the normal propagators in the second diagram in Fig. 1(a), $G(\epsilon_p, i\omega_n) = (i\omega_n - \epsilon_p)^{-1}$, one gets

$$\delta V^{n,n'}_{p,p'} = \frac{1}{2} V_{p,p'}(0)^2 \sum_{\mathbf{p}'_1} \theta(\omega_c - |\epsilon_{p_1}|)\theta(\omega_c - |\epsilon_{p'_1}|) \times \frac{\tanh(\epsilon_{p_1}/2T) - \tanh(\epsilon_{p'_1}/2T)}{i\nu_{n+n'} + \epsilon_{p_1} - \epsilon_{p'_1}}, \quad (8)$$

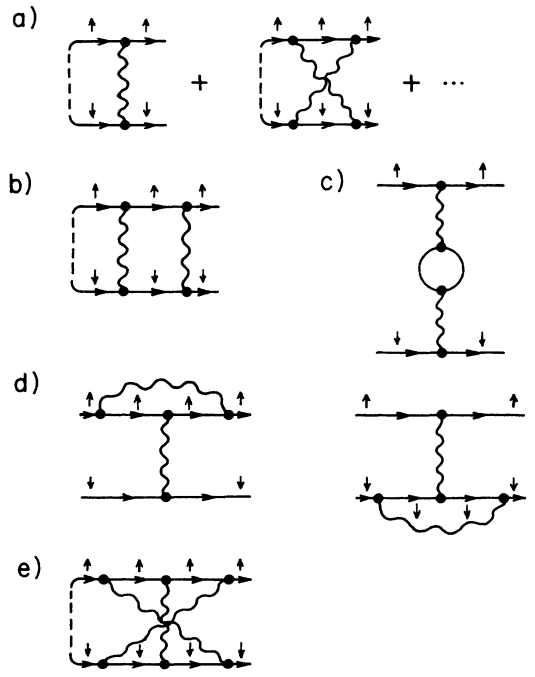

FIG. 1. The lowest-order diagrams for a general BCS type interaction. A dashed line indicates how to generate the corresponding graph for the anomalous self-energy. In the text we explain which of the diagrams (a)–(d) contribute for the interaction given by Eq. (2). The diagram (e) is of the order of $\lambda^3\omega_c^3/E_F^2$ in three-dimensional case and is omitted in our consideration (see Ref. 15).

where $\mathbf{p}+\mathbf{p}' = \mathbf{p}_1+\mathbf{p}'_1$ and $i\nu_n = i\pi T 2n$ is a boson Matsubara frequency. It is easy to see that Eqs. (4), (7), and (8) imply $\Delta_p = \Delta\theta(\omega_c - |\epsilon_p|)$, and upon carrying the sums in the second term in (7) one finds that only $\mathrm{Re}\delta V^{n,n'}_{p,p'}$ contributes. It is important to note that $\mathrm{Re}\delta V^{n,n'}_{p,p'}$ is always positive and therefore the second term in Eq. (7) has the sign opposite to the first term. As a result, $\delta V^{n,n'}_{p,p'}$ will cause a *reduction* of T_c. The equation for the critical temperature can be written in the following form (see Appendix A)

$$1 = \Lambda(T_c) - \lambda\frac{\omega_c}{E_F}\,\Lambda(T_c)^2\kappa(T_c)\,, \tag{9}$$

where

$$\Lambda(T) = \lambda\int_0^{\omega_c}\frac{d\epsilon}{\epsilon}\tanh\frac{\epsilon}{2T}\,, \tag{10}$$

and $\kappa(T)$ is a universal function of $\omega_c/\pi T$ defined in the Appendix A. $\kappa(T)$ as a function of T/T_c^{BCS}, where T_c^{BCS} is the solution of the BCS equation $\Lambda(T_c^{\mathrm{BCS}}) = 1$ is shown in Fig. 2 for several values of λ. The interesting feature of $\kappa(T)$ is a very slow change near T_c^{BCS} and a rapid variation in the vicinity of $T = 0$. From Eq. (9) it is clear that for a fixed λ the critical temperature is a decreasing function of ω_c/E_F. This is illustrated in Fig. 3 for various values of λ. At small ω_c/E_F the rate of decrease in T_c/T_c^{BCS} does not depend much on λ. However, when ω_c/E_F is not very small compared to 1, T_c/T_c^{BCS} decreases more rapidly with increasing λ. The equation for T_c, Eq. (9), is quadratic in $\Lambda(T_c)$ and it is easy to see that for a fixed λ the solution exists only for values of ω_c/E_F smaller than some critical value $(\omega_c/E_F)_c$. Moreover, there are two solutions (the lower ones are given by the dashed lines in Fig. 3), which approach each other as ω_c/E_F is increased and eventually coincide at $(\omega_c/E_F)_c$.

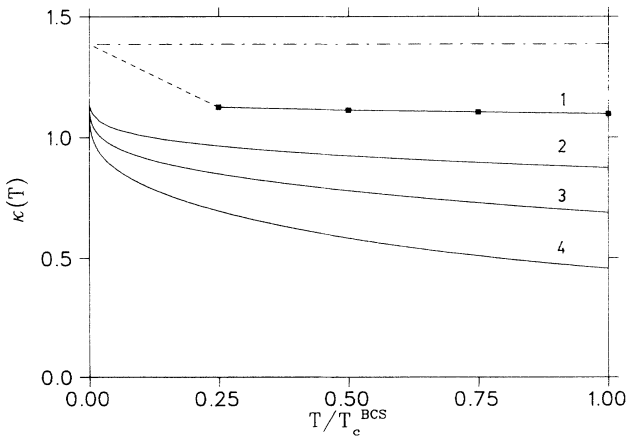

FIG. 2. The function $\kappa(T)$ for different λ's. Curve (1) is for $\lambda = 0.1$, curve (2) is for $\lambda = 0.2$, curve (3) is for $\lambda = 0.3$, and curve (4) is for $\lambda = 0.5$. The dot-dashed line gives the analytic limit of $\kappa(T)$ when $\lambda \to 0$. The computing time for $T/T_c < 0.25$ with $\lambda = 0.1$ became prohibitively long, and the dashed line just indicates that the curve continues down to the analytic result at $T \to 0$.

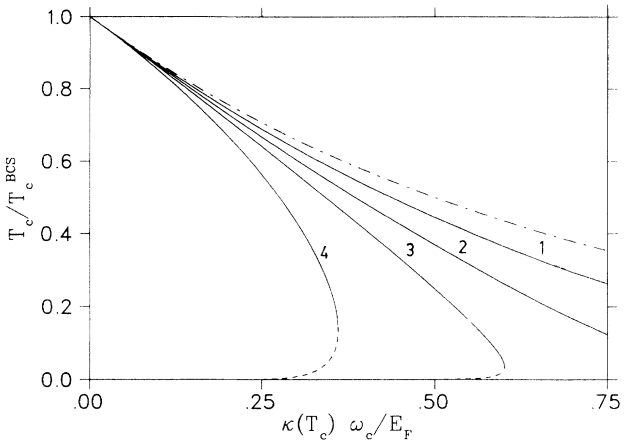

FIG. 3. The superconducting critical temperatures calculated from Eq. (9) for different values of λ. Curve (1) is for $\lambda = 0.1$, curve (2) is for $\lambda = 0.2$, curve (3) is for $\lambda = 0.3$, curve (4) is for $\lambda = 0.5$. The dashed lines give the lower of the two solutions of Eq. (9). The dot-dashed line gives the analytic limit of the critical temperature when $\lambda \to 0$.

The larger of the two solutions is the physical T_c. It is necessary to emphasize that although the correction to the BCS term, $\Lambda(T_c)$, in Eq. (9) is of the order of $\lambda\omega_c/E_F$, the correction to T_c is much larger due to exponential dependence of T_c on the correction term, which is implied by Eqs. (9) and (10).

One could argue that the effect of vertex corrections on the superconducting transition temperature might not be qualitatively correct within the BCS treatment, since the changes in the normal (i.e., diagonal) self-energy due to vertex corrections with a retarded interaction (e.g., a reduction in the renormalization function[15]) could have an important effect. In the BCS treatment only the modifications of the pairing self-energy are present. In the next section we address the problem of modifying the usual Eliashberg theory of superconducting T_c (Ref. 3) to include the effect of vertex corrections.

III. ELIASHBERG EQUATIONS FOR T_c AND HIGHER-ORDER ELECTRON SELF-ENERGY DIAGRAMS

In this section we use the Nambu formalism of the strong-coupling theory[16,4] to obtain the T_c equation, which includes the effect of the lowest-order vertex correction. The (2×2)-matrix irreducible electron self-energy could be written as

$$\hat{\Sigma}(\mathbf{k}, i\omega_n) = \hat{\Sigma}_N(\mathbf{k}, i\omega_n) + \hat{\Sigma}_A(\mathbf{k}, i\omega_n)\,, \tag{11}$$

where

$$\hat{\Sigma}_N(\mathbf{k}, i\omega_n) = i\omega_n\big[1 - Z_n(\mathbf{k})\big]\hat{\tau}_0 + \chi_n(\mathbf{k})\hat{\tau}_3 \tag{12}$$

is the normal part and

$$\hat{\Sigma}_A(\mathbf{k}, i\omega_n) = Z_n(\mathbf{k})\big[\Delta_n(\mathbf{k})\hat{\tau}_1 + \bar{\Delta}_n(\mathbf{k})\hat{\tau}_2\big] \tag{13}$$

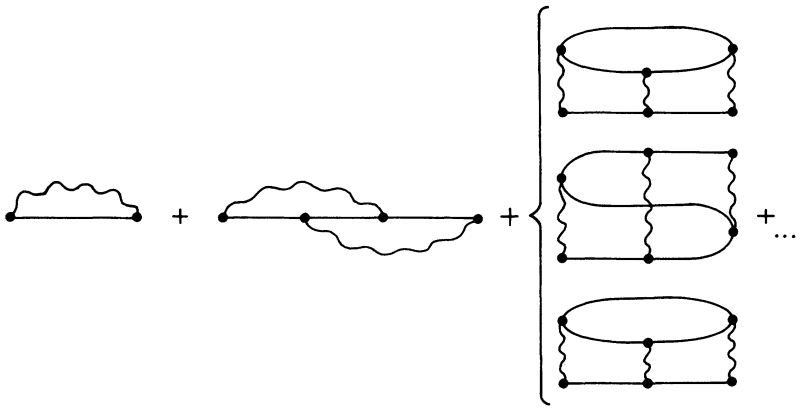

FIG. 4. The lowest-order skeleton diagrams for the electron self-energy. The order of magnitude of the diagram with two crossed boson lines is $\lambda^2\omega_c^2/E_F$ in the three-dimensional isotropic case and $\lambda^2\omega_c^2\ln(E_F/\omega_c)/E_F$ in two-dimensional isotropic case. Here λ is the coupling constant defined as twice the first inverse moment of the boson spectral function, and ω_c is the characteristic frequency of boson spectral function (it is assumed that $\omega_c \ll E_F$). The order of magnitude of the skeleton diagrams with three boson lines is $\lambda^3\omega_c^3/E_F^2$ in three-dimensional isotropic case and $\lambda^2\omega_c^2/E_F$ in two-dimensional isotropic case.

is the anomalous part. Here, $Z_n(\mathbf{k})$ is the renormalization function, $\chi_n(\mathbf{k})$ is the shift of the chemical potential, $\Delta_n(\mathbf{k})$ and $\bar{\Delta}_n(\mathbf{k})$ are the real and the imaginary parts of the gap function (renormalized pairing self-energy), and $\hat{\tau}_0, \hat{\tau}_1, \hat{\tau}_2, \hat{\tau}_3$ are the Pauli matrices.[3,4,16] The diagrams for $\hat{\Sigma}(\mathbf{k}, i\omega_n)$ are shown in Fig. 4, where the solid lines denote the dressed (2×2)-matrix electron Green's function $\hat{G}(\mathbf{k}, i\omega_n)$ and the wavy lines denote the dressed boson (phonon or spin-fluctuation) propagators. At temperatures $T \approx T_c$ the pairing self-energy becomes vanishingly small, and one can retain only the terms that are linear in the pairing self-energy. Then, the normal and the anomalous part of $\hat{G}(\mathbf{k}, i\omega_n) = \hat{G}_N(\mathbf{k}, i\omega_n) + \hat{F}(\mathbf{k}, i\omega_n)$ could be written as

$$\hat{G}_N(\mathbf{k}, i\omega_n) = Z_n(\mathbf{k})^{-1}\frac{i\omega_n\hat{\tau}_0 + \tilde{\epsilon}_n(\mathbf{k})\hat{\tau}_3}{(i\omega_n)^2 - [\tilde{\epsilon}_n(\mathbf{k})]^2}, \tag{14}$$

$$\hat{F}(\mathbf{k}, i\omega_n) = Z_n(\mathbf{k})^{-1}\frac{\Delta_n(\mathbf{k})\hat{\tau}_1 + \bar{\Delta}_n(\mathbf{k})\hat{\tau}_2}{(i\omega_n)^2 - [\tilde{\epsilon}_n(\mathbf{k})]^2}, \tag{15}$$

respectively. Here, $\tilde{\epsilon}_n(\mathbf{k})$ is the renormalized electronic spectrum

$$\tilde{\epsilon}_n(\mathbf{k}) = Z_n(\mathbf{k})^{-1}\left[\epsilon_{\mathbf{k}} + \chi_n(\mathbf{k})\right]. \tag{16}$$

The usual approximation for the electron self-energy in the case of interaction with phonons and/or spin fluctuations is to keep only the contribution of the first diagram in Fig. 4,

$$\hat{\Sigma}^{(1)}(\mathbf{k}, i\omega_n) = -T\sum_{n'}\sum_{\mathbf{k}'}\left\{\begin{array}{c} D(\mathbf{k}-\mathbf{k}', i\nu_{n-n'}) \\ -P_s(\mathbf{k}-\mathbf{k}', i\nu_{n-n'}) \end{array}\right\}\left\{\begin{array}{c}\hat{\tau}_3 \\ \hat{\tau}_0\end{array}\right\}\hat{G}(\mathbf{k}', i\omega_{n'})\left\{\begin{array}{c}\hat{\tau}_3 \\ \hat{\tau}_0\end{array}\right\}. \tag{17}$$

In Eq. (17), the upper line in all curly brackets corresponds to the electron-phonon interaction and the lower line to the electron-spin-fluctuation interaction. The phonon propagator D can be written in the form

$$D(\mathbf{q}, i\nu_m) = N(0)^{-1}\int_0^\infty d\Omega B(\mathbf{q}, \Omega)\frac{2\Omega}{(i\nu_m)^2 - \Omega^2}, \tag{18}$$

where $B(\mathbf{q}, \Omega)$ is the phonon spectral weight. The spin-fluctuation propagator P_s is defined through a summation of an infinite series of diagrams involving the irreducible particle-hole interaction,[17] and could be expressed in terms of the spin susceptibility $\chi_s(\mathbf{q}, \omega)$

$$P_s(\mathbf{q}, i\nu_m) = \frac{3}{2}U^2\chi_s(\mathbf{q}, i\nu_m) = -\frac{3U^2}{2\pi}\int_{-\infty}^{+\infty} d\omega\frac{\mathrm{Im}\chi_s(\mathbf{q}, \omega)}{i\nu_m - \omega}, \tag{19}$$

where U is the interaction constant.[17] As is well known, the accuracy of the approximation $\hat{\Sigma}(\mathbf{k}, i\omega_n) = \hat{\Sigma}^{(1)}(\mathbf{k}, i\omega_n)$ in the case of electrons interacting with phonons in a three-dimensional system is $O(\omega_c^2/E_F)$, where ω_c is a typical phonon energy;[18,19] in a quasi-two-dimensional case the accuracy is $O[(\omega_c^2/E_F)\ln(E_F/\omega_c)]$.[20] Similar estimates apply to the effective electron spin-fluctuation interaction, with ω_c a typical spin-fluctuation energy, when $\chi_s(\mathbf{q}, \omega)$ is *isotropic*,[21] and since in that case the spin-fluctuation spectral function tails off up to $8E_F$, the approximation is highly suspect.

The second diagram in Fig. 4 represents the first-order vertex correction in the electron-phonon problem. Also, it is possible to sum certain infinite subsets of diagrams involving the irreducible particle-hole interaction U, and cast the result in the form of a diagram with crossing spin-fluctuation lines.[21] However, the diagrammatic rules with spin-fluctuation propagators have to be augmented by introducing an additional multiplicative factor α_s, which takes into account all relevant combinations of ladders and strings of bubbles with the irreducible particle-hole interaction, as well as the definition (19) of the spin-fluctuation propagator (see Sec. III B). The contribution of the self-energy diagram with two crossed boson lines for both cases can be written as

$$\hat{\Sigma}^{(2)}(\mathbf{k}, i\omega_n) = T^2 \sum_{n'n''} \sum_{\mathbf{k}'\mathbf{k}''} \left\{ \begin{array}{c} D(\mathbf{k}-\mathbf{k}', i\nu_{n-n'}) D(\mathbf{k}-\mathbf{k}'', i\nu_{n-n''}) \\ \alpha_s P_s(\mathbf{k}-\mathbf{k}', i\nu_{n-n'}) P_s(\mathbf{k}-\mathbf{k}'', i\nu_{n-n''}) \end{array} \right\}$$
$$\times \left\{ \begin{array}{c} \hat{\tau}_3 \\ \hat{\tau}_0 \end{array} \right\} \hat{G}(\mathbf{k}', i\nu_{n'}) \left\{ \begin{array}{c} \hat{\tau}_3 \\ \hat{\tau}_0 \end{array} \right\} \hat{G}(\mathbf{k}'+\mathbf{k}''-\mathbf{k}, i\nu_{n'+n''-n}) \left\{ \begin{array}{c} \hat{\tau}_3 \\ \hat{\tau}_0 \end{array} \right\} \hat{G}(\mathbf{k}'', i\nu_{n''}) \left\{ \begin{array}{c} \hat{\tau}_3 \\ \hat{\tau}_0 \end{array} \right\} . \tag{20}$$

In this case (two crossed spin-fluctuation lines) $\alpha_s = 1/3$. It is important to note that the second-order diagram $\Sigma^{(2)}(\mathbf{k}, i\omega_n)$ is related to an intermediate electron propagator $G(\mathbf{k}', i\omega_{n'})$ through the kernel that depends not only on $n - n'$ [as in the case of $\Sigma^{(1)}(\mathbf{k}, i\omega_n)$, Eq. (17)] but also on n.

A. Isotropic electron-phonon interaction

We consider first the case of isotropic electron-phonon interaction for two- and three- dimensional electron gas. It will be assumed that the $\mathbf{q}$ dependence of the spectral weight $B(\mathbf{q}, \Omega)$ is negligible, and we replace $B(\mathbf{q}, \Omega)$ by the Eliashberg function $\alpha^2 F(\Omega)$. In the case of isotropic interaction the renormalization function $Z_n(\mathbf{k})$ and the shift of the chemical potential $\chi_n(\mathbf{k})$ depend on $\mathbf{k}$ via ϵ_k. We assume a symmetric band $-E_F < \epsilon_k < E_F$, with $\epsilon_k = -k^2/2m + E_F$, in which case $\chi_n(\mathbf{k}) \sim O(\omega_c^3/E_F^2)$ and could be ignored within the accuracy $O(\omega_c^2/E_F)$. One then obtains from (17) and (20) the following equations for the self-energies

$$\hat{\Sigma}^{(1)}(i\omega_n) = T \sum_{n'} \lambda(n-n') \int_{-E_F}^{E_F} d\epsilon_{k'} \hat{\tau}_3 \hat{G}(\epsilon_{k'}, i\omega_{n'}) \hat{\tau}_3 ,$$
$$\hat{\Sigma}^{(2)}(\epsilon_k, i\omega_n) = \frac{T^2}{4E_F} \sum_{n'n''} \lambda(n-n')\lambda(n-n'') \int_{-E_F}^{E_F} d\epsilon_{k'} \int_{-E_F}^{E_F} d\epsilon_{k'''} \int_{-E_F}^{E_F} d\epsilon_{k''}$$
$$\times M(k, k'''; k', k'') \hat{\tau}_3 \hat{G}(\epsilon_{k'}, i\omega_{n'}) \hat{\tau}_3 \hat{G}(\epsilon_{k'''}, i\omega_{n'+n''-n}) \hat{\tau}_3 \hat{G}(\epsilon_{k''}, i\omega_{n''}) \hat{\tau}_3 , \tag{21}$$

where $\lambda(m)$ is defined in the usual way

$$\lambda(m) = \int_0^\infty d\Omega \alpha^2 F(\Omega) \frac{2\Omega}{\nu_m^2 + \Omega^2} . \tag{22}$$

All momenta $k^{(i)}$ in Eqs. (21) are functions of the corresponding energies $\epsilon_{k^{(i)}}$ and the function $M(k, k'''; k', k'')$ is determined by the dimensionality of the system

$$M(k, k'''; k', k'') = \theta(Q_M - Q_m) \int_{Q_m}^{Q_M} dQ \times \left\{ \begin{array}{ll} 1/2k & \text{(3D)} \\ k_F^2 \pi^{-2} 2Q X(k, k''', Q)^{-1} X(k', k'', Q)^{-1} & \text{(2D)} . \end{array} \right. \tag{23}$$

Here $Q_M = \min(k + k''', k' + k'')$, $Q_m = \max(|k - k'''|, |k' - k''|)$, and $X(k, k', Q)^2 = [Q^2 - (k - k')^2][(k + k')^2 - Q^2]$ is biquadratic and symmetric under the exchange of any pair of variables. As in the BCS case (see Appendix A), the function $M(k, k'''; k', k'')$ is approximated by its value near the Fermi surface

$$M(k, k'''; k', k'') = \left\{ \begin{array}{ll} 1 & \text{(3D)} \\ 3\pi^{-2} \ln[8E_F / \sqrt[3]{|P(\epsilon_k, \epsilon_{k'''}, \epsilon_{k'}, \epsilon_{k''})|}] & \text{(2D)} , \end{array} \right. \tag{24}$$

with $P(\epsilon_1, \epsilon_2, \epsilon_3, \epsilon_4) = (\epsilon_1 + \epsilon_2 - \epsilon_3 - \epsilon_4)(\epsilon_1 - \epsilon_2 + \epsilon_3 - \epsilon_4)(\epsilon_1 - \epsilon_2 - \epsilon_3 + \epsilon_4)$. Although in the present case—in contrast to the BCS-type interaction—not all momenta are near the Fermi surface, this approximation could be justified for the same reasons as in the normal state.[22] One can see that after such an approximation $\hat{\Sigma}^{(2)}(\epsilon_k, i\omega_n)$ does not depend on ϵ_k in three dimensions (3D). In two dimensions (2D) the dependence on ϵ_k is only through logarithms that have a reducing prefactor T/E_F (see Appendix B). After equating the coefficients of various Pauli matrices on both sides of the equation for $\hat{\Sigma}^{(1)}(i\omega_n) + \hat{\Sigma}^{(2)}(i\omega_n)$, which is implied by Eqs. (21), one finds the strong-coupling equations corrected by the second-order diagram

$$Z_n = 1 + \frac{\pi T}{|\omega_n|} \sum_{n'} \lambda(n-n') A(n, n') s_n s_{n'} a_{n'} , \tag{25}$$

$$Z_n \Delta_n = \pi T \sum_{n'} \left[\lambda(n-n') B(n, n') + C(n, n') \right] a_{n'} \frac{\Delta_{n'}}{|\omega_{n'}|} . \tag{26}$$

The equation for $\bar{\Delta}_n$ is the same as the equation for Δ_n, and could be suppressed. The factors $a_n = (2/\pi) \arctan(E_F / Z_n |\omega_n|)$ result from integrations over ϵ_k's in Eqs. (21) and $s_n = \mathrm{sgn}(\omega_n)$. In 3D the matrices $A(n, n')$, $B(n, n')$, and $C(n, n')$ are

$$A(n,n') = 1 - \frac{\pi^2 T}{4E_F} \sum_{n''} \lambda(n-n'') s_{n'+n''-n} s_{n''} a_{n'+n''-n} a_{n''} , \tag{27}$$

$$B(n,n') = 1 - \frac{\pi^2 T}{2E_F} \sum_{n''} \lambda(n-n'') s_{n'+n''-n} s_{n''} a_{n'+n''-n} a_{n''} , \tag{28}$$

$$C(n,n') = \frac{\pi^2 T}{4E_F} \sum_{n''} \lambda(n-n'')\lambda(n'-n'') s_{n'-n''+n} s_{n''} a_{n'-n''+n} a_{n''} . \tag{29}$$

The second term in matrix $A(n,n')$ is due to a vertex correction contribution to the diagonal (i.e., normal) part of the self-energy. Since near T_c it is sufficient to keep the diagrams for the pairing self-energy in which the anomalous Green's function $\hat{F}(\mathbf{k}, i\omega_n)$ appears only once, there are only three vertex correction diagrams that contribute. The second term in matrix $B(n,n')$ corresponds to the sum of the contributions from the second-order graph when the anomalous function $\hat{F}(\mathbf{k}, i\omega_n)$ is taken for the first electron line or the third electron line in a diagram with two crossed boson lines. The matrix $C(n,n')$ corresponds to the contribution from the second-order graph when the anomalous function $\hat{F}(\mathbf{k}, i\omega_n)$ is taken for the middle line in such a diagram. We note that the usual Eliashberg equations are obtained from Eqs. (25)–(29) by taking the limit $E_F \to \infty$.

The solutions of the T_c equations for the Einstein model $\alpha^2 F(\Omega) = \lambda \Omega_E / 2\delta(\Omega - \Omega_E)$, with $\Omega_E = 10$ meV, are shown in Fig. 5. As in the case of the BCS model, Sec. II, the critical temperature T_c decreases with increasing Ω_E/E_F. However, in the strong-coupling case the T_c is suppressed at a slower rate, presumably due to a reduction of the renormalization function Z_n by the lowest-order vertex correction. This effect is absent in the BCS case. To illustrate the effect of the lowest-order vertex correction on T_c for a realistic spectrum $\alpha^2 F(\Omega)$ we solved Eqs. (25) and (26) for Pb.[23] The maximum energy of the spectrum is $\Omega_{\max} = 11.1$ meV, and the electron-phonon coupling parameter $\lambda \equiv 2\int_0^\infty d\Omega \alpha^2 F(\Omega)/\Omega$ is equal to 1.55. It is easy to include the usual Coulomb graph into the theory and describe it in terms of the pseudopotential μ^*.[3,4] We have chosen $\mu^* = 0.136$ for the cutoff of 55 meV in the sums over Matsubara frequencies so that the T_c is 7.2 K for $E_F \to \infty$ (the usual case). The results (full squares in Fig. 5) are very similar to the results obtained for the Einstein model. It is interesting to note that for $E_F = 9.47$ eV, which is the free-electron-gas value for the Fermi energy in Pb,[24] the correction to T_c is about 0.2%.

Finally in this subsection we consider the correction to the critical temperature for the spectrum which, like the spin-fluctuation spectrum in an *isotropic* system, is linear in Ω at small energies and has a long $1/\Omega$-tail at high energies. Namely, we take

$$\alpha^2 F(\Omega) = \frac{\lambda}{4}\left[\frac{\Omega}{\omega_0}\theta(\omega_0 - \Omega) + \frac{\omega_0}{\Omega}\theta(\Omega - \omega_0)\theta(\omega_{\max} - \Omega)\right] \Big/ \left[1 - \frac{\omega_0}{2\omega_{\max}}\right]. \tag{30}$$

The relative changes of T_c calculated from Eqs. (25) and (26) compared to T_c^E calculated from the usual Eliashberg equations at different ratios $\bar{\omega}_{\ln}/E_F$ and $\bar{\omega}/E_F$ are shown in Fig. 6. Here, $\bar{\omega}_{\ln}$ is the logarithmically averaged frequency and $\bar{\omega}$ is the average frequency,

$$\ln \bar{\omega}_{\ln} = \frac{2}{\lambda}\int_0^{\omega_{\max}} d\Omega \frac{\alpha^2 F(\Omega)}{\Omega} \ln \Omega \tag{31}$$

$$\bar{\omega} = \int_0^{\omega_{\max}} d\Omega \alpha^2 F(\Omega)\Omega \Big/ \int_0^{\omega_{\max}} d\Omega \alpha^2 F(\Omega) . \tag{32}$$

Note that the area under spectral function (30) increases logarithmically with increasing $\omega_{\max}$, but the average frequency is approximately proportional to $\omega_{\max}$ (for $\omega_0 \ll \omega_{\max}$ one can find $\bar{\omega} \approx \omega_{\max}/\ln(\omega_{\max}/\omega_0)$ and $\bar{\omega}_{\ln} \approx \omega_0$). We choose $\lambda = 1$, $\omega_0 = 10$ meV, $\omega_{\max} = 500$ meV and the cut off in the sums over Matsubara frequencies is $5\omega_{\max}$. For these values of parameters $\bar{\omega}_{\ln} = 9.43$ meV, $\bar{\omega} = 111.8$ meV, and $T_c^E = 37.2$ K.

B. Highly anisotropic electron-boson interaction

As an example of a highly anisotropic electron-boson interaction, we consider a model of a spin-fluctuation mediated superconductivity, which is analogous to the models proposed to explain the superconductivity in copper-oxides.[25,26,10] To evaluate the second-order correction graph for the self-energy due to the exchange of spin-fluctuations, we use a model in which the irreducible particle-hole interaction is taken to have a contact form and magnitude U.[17] The first-order graph can be obtained in the usual way (see Fig. 6) by combining the contribution from the strings of bubbles and ladders.[17] In evaluating the contribution from these diagrams in the superconducting state we use Gor'kov's diagrammatic method[1] due to the appearance of different boson lines in the normal and the anomalous channel: the line that corresponds to the ladders (t), the line with odd numbers of bubbles (l_1), and the line with even numbers of bubbles (l_2). After making the usual approximation for these lines[21] one gets the expression for the self-energy

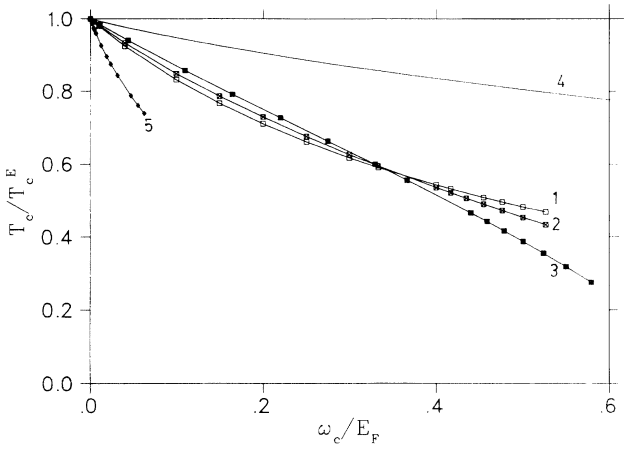

FIG. 5. The relative changes of the superconducting critical temperature calculated from Eqs. (25) and (26), which include the lowest-order vertex correction, compared to the temperature T_c^E calculated from the usual Eliashberg equations for different spectral functions $\alpha^2F(\Omega)$. Curves (1) and (2) are for the Einstein model with $\Omega_E = 10$ meV and $\lambda = 0.5$, $\mu^* = 0.0$, $T_c^E = 4.57$ K for curve (1), and $\lambda = 1.0$, $\mu^* = 0.0$, $T_c^E = 13.28$ K for curve (2). For these two curves ω_c is Ω_E. Curve (3) is for the spectral function of Pb: $\lambda = 1.55$, $\mu^* = 0.136$, $\Omega_{\max} = 11.1$ meV, and $T_c^E = 7.19$ K. For this curve ω_c is $\Omega_{\max}$. Curves (4) and (5) are for the spectral function given by Eq. (30) with $\lambda = 1.0$, $\mu^* = 0.0$, $T_c^E = 15.3$ K. For curve (4) $\omega_c = \bar{\omega}$ and for curve (5) $\omega_c = \bar{\omega}_{\ln}$ (see the text).

that could be written in the Nambu notation [the lower line in curly brackets in Eq. (17)]. It is possible to sum several infinite series of diagrams for the normal and the anomalous self-energy and cast them into the form of diagrams with two crossing spin-fluctuation lines. All possible diagrams of this type are shown in Fig. 7. With the same approximations for the propagators t, l_1, and l_2 as in the first order graph, one can write the contribution of all diagrams in Fig. 7 in the form given by Eq. (20) with $\alpha_s = 1/3$. In numerical calculations we will treat α_s as a free parameter ($\leq 1/3$), which will allow us to control the relative contribution of the second-order graph.

We consider a model of electrons moving on a square lattice with a dispersion

$$\epsilon_{\mathbf{k}} = -2t[\cos(k_x a) + \cos(k_y a)] - \mu\,, \tag{33}$$

where a is the lattice constant, t is the hopping matrix element, and μ is the chemical potential. The wave vector $\mathbf{k}$ runs through the first Brillouin zone ($-\pi/a < k_x < \pi/a$, $-\pi/a < k_y < \pi/a$). For the spin-susceptibility we adopt a model that gives very sharp peaks in the momentum space at the four corners of the Brillouin zone,[25]

$$\chi_s(\mathbf{q}, i\nu_m) = \chi_\Gamma \int_0^\infty d\Omega P(\Omega) \frac{2\Omega}{\nu_m^2 + \Omega^2} \times \frac{1}{a^2} \sum_{\mathbf{Q}} \frac{\Gamma}{(q_x - Q_x)^2 + \Gamma^2} \frac{\Gamma}{(q_y - Q_y)^2 + \Gamma^2}\,. \tag{34}$$

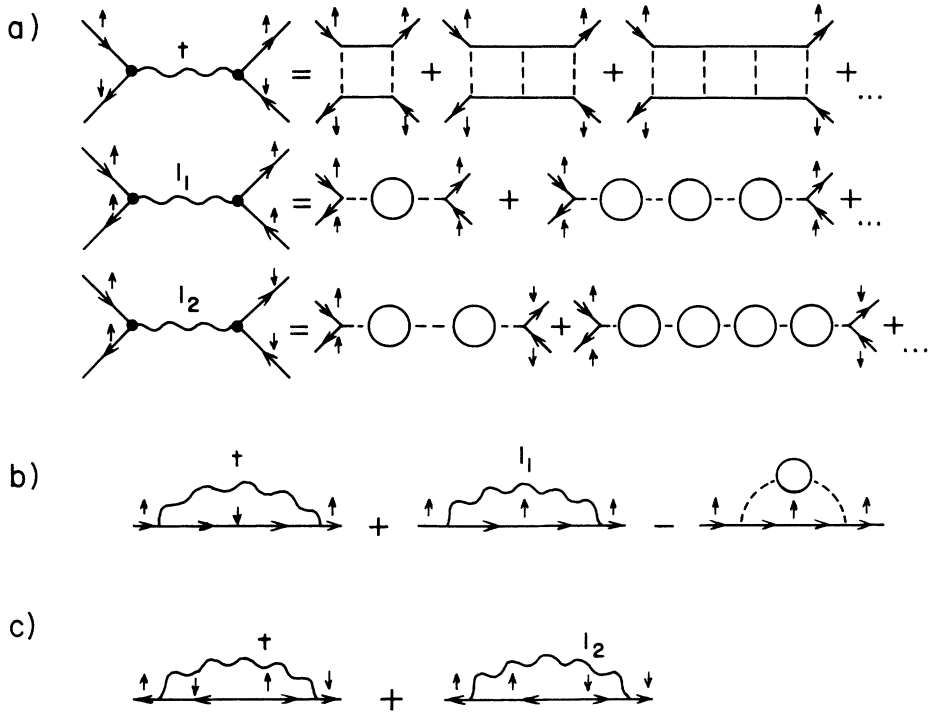

FIG. 6. (a) The random-phase-approximation summation of the diagrams contributing to the interaction arising from the exchange of transverse spin-fluctuation (line t) and from the exchange of longitudinal spin-fluctuation with odd (line l_1) and even (line l_2) numbers of bubbles. (b) The contribution to the normal irreducible self-energy from the first-order spin-fluctuation exchange. The third diagram is subtracted to prevent double counting, since it is a part of both t and l_1. (c) The contribution to the anomalous self-energy from the first-order spin-fluctuation exchange.

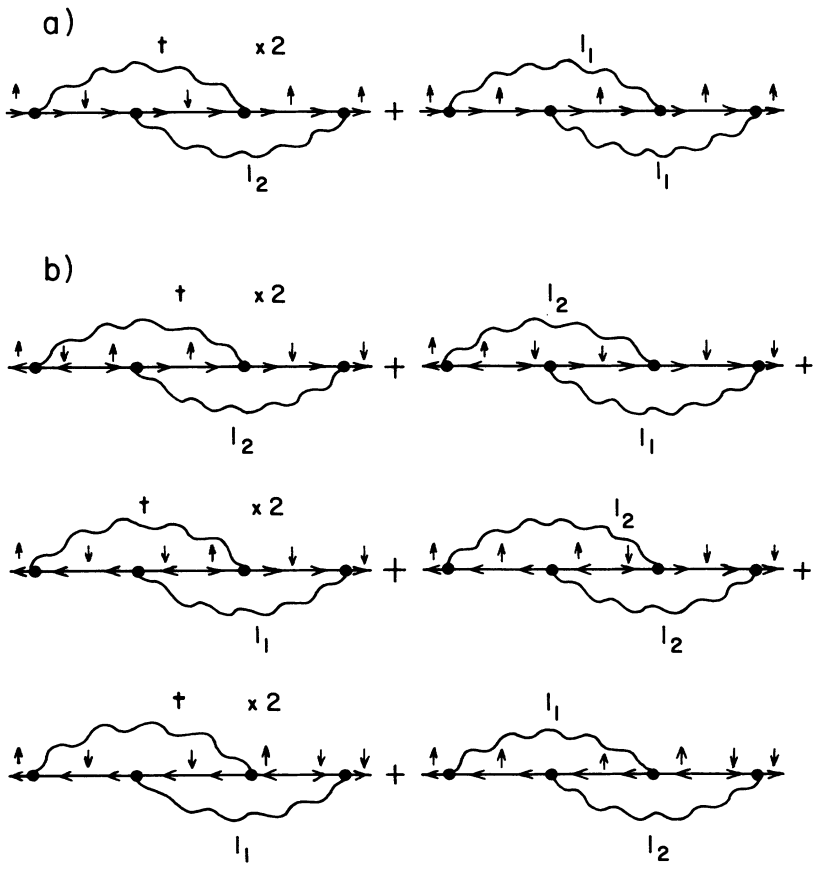

FIG. 7. (a) The second-order spin-fluctuation contribution to the normal self-energy near T_c. (b) The second-order spin-fluctuation contribution to the anomalous self-energy near T_c. Some diagrams appear twice, since the exchange between different boson lines gives topologically distinct diagrams, which have the same contribution.

Here $P(\Omega)$ is the spectral function analogous to the Eliashberg function in the isotropic case. For convenience $P(\Omega)$ is normalized such that $\int_0^\infty d\Omega P(\Omega) = 1$. The sum over $\mathbf{Q} = (\pm\pi/a, \pm\pi/a)$ is the sum over the positions of four peaks in the spin susceptibility at the corners of the square Brillouin zone. We will assume that the four peaks are sharp enough so that in a product of spin susceptibility with any other smooth function of momentum only the values of this function at the corners of the Brillouin zone are taken into account. Formally this is expressed by replacing the sharp peaks with δ functions, i.e., by taking the limit $\Gamma \to 0$. We note that this is purely a formal device, since this limit corresponds physically to an infinite antiferromagnetic correlation length. The δ-function approximation will, however, simplify several integrations over momenta which appear in the expressions for the contributions of the first- and the second-order graph to the self-energy. It should be noted that this model of four δ peaks in the corners of a square Brillouin zone implies the $\epsilon_{\mathbf{k}}$ and ω dependence of the normal-state self-energy $\Sigma(\epsilon_{\mathbf{k}}, \omega)$, which is qualitatively different from the one found in the isotropic case.[27]

The self-consistent equations for the superconducting critical temperature based on the first-order self-energy graph take the form

$$Z_n(\mathbf{k}) = 1 + \frac{\pi T}{|\omega_n|} \sum_{n'} \frac{1}{4} \sum_{\mathbf{Q}} \lambda_s(n-n') G_{n'}(\mathbf{k}+\mathbf{Q}) s_n s_{n'} , \tag{35}$$

$$Z_n(\mathbf{k})\Delta_n(\mathbf{k}) = -\pi T \sum_{n'} \frac{1}{4} \sum_{\mathbf{Q}} \lambda_s(n-n') \times G_{n'}(\mathbf{k}+\mathbf{Q}) \frac{\Delta_{n'}(\mathbf{k}+\mathbf{Q})}{|\omega_{n'}|} , \tag{36}$$

where

$$G_n(\mathbf{k}) = Z_n(\mathbf{k})^{-1} \frac{|\omega_n|}{\omega_n^2 + \tilde{\epsilon}_n(\mathbf{k})^2} \tag{37}$$

and

$$\lambda_s(n-n') = \frac{3}{\pi} g^2 \int_0^\infty d\Omega P(\Omega) \frac{\Omega}{\nu_{n-n'}^2 + \Omega^2} . \tag{38}$$

Here $g^2 = U^2 \chi_\Gamma$. Note that $\lambda_s(n-n')$ has the units of energy. In the following we neglect the difference between the renormalized spectrum $\tilde{\epsilon}_n(\mathbf{k})$ and $\epsilon_{\mathbf{k}}$. It is assumed that this approximation is not critical for the present study of the effect of higher-order self-energy diagrams on T_c.[28]

The sign in Eq. (36) can be changed by the appropriate choice of the symmetry of the order parameter

$$\Delta_n(\mathbf{k}) = \Delta_n^\alpha(\mathbf{k})[\cos(k_x a) + \alpha \cos(k_y a)] , \tag{39}$$

where $\alpha = \pm 1$. For both $\alpha = 1$ (extended s wave) and $\alpha = -1$ (d wave) the T_c equations are the same. We assume that $Z_n(\mathbf{k})$ and $\Delta_n^\alpha(\mathbf{k})$ depend on momentum through $\epsilon_{\mathbf{k}}$. Thus, the momentum dependence enters Eqs. (35) and (36) only through $\epsilon_{\mathbf{k}}$ or $\epsilon_{\mathbf{k}+\mathbf{Q}} = -\epsilon_{\mathbf{k}} - 2\mu$.

Because of the periodicity of the electronic spectrum,

$$\epsilon_{\mathbf{k}+m\mathbf{Q}} = \begin{cases} -\epsilon_{\mathbf{k}} - 2\mu & m \text{ is odd} \\ \epsilon_{\mathbf{k}} & m \text{ is even}, \end{cases} \tag{40}$$

it is clear that the functions $Z_n(\mathbf{k}+\mathbf{Q})$ and $\Delta_n(\mathbf{k}+\mathbf{Q})$ are given by the equations that have the same form as Eqs. (35) and (36), except that all the functions on the right-hand side depend on $\mathbf{k}$ (instead of $\mathbf{k}+\mathbf{Q}$). In the following the sums over $\mathbf{Q}$ are omitted and $\mathbf{Q} = (\pi/a, \pi/a)$.

It is interesting to compare Eqs. (35) and (36) with Eliashberg equations in the isotropic case. The main difference is in the presence of temperature dependent factors $G_n(\mathbf{k})$ coming from the Green's functions after integration over the momenta. In order to get more insight one can take the BCS limit by using the square-well model[29] to approximate the kernel:

$$\lambda(n-n') = \lambda\theta(\omega_c - |\omega_n|)\theta(\omega_c - |\omega_{n'}|).$$

In the isotropic case for $\omega_c \gg \pi T_c$ this approximation leads to the BCS formula $T_c = (2\gamma/\pi)\omega_c e^{-1/\lambda}$. In the case of four δ peaks in the corners of the Brillouin zone the square-well approximation

$$\lambda_s(n-n') = \lambda_s\theta(\omega_c - |\omega_n|)\theta(\omega_c - |\omega_{n'}|)$$

in Eqs. (35) and (36) gives the following T_c equation for $\omega_c \gg \pi T_c$:

$$\frac{\pi\lambda_s}{2\mu}\tanh\frac{\mu}{2T_c} = 1\,. \tag{41}$$

There are two important implications of this equation. First, the solution does not exist for arbitrary λ_s. The inequality $\lambda_s > 2|\mu|/\pi$ must be satisfied. Second, for $\lambda_s \gg |\mu|$ the superconducting critical temperature is proportional to the interaction constant: $T_c \simeq \pi\lambda_s/4$.

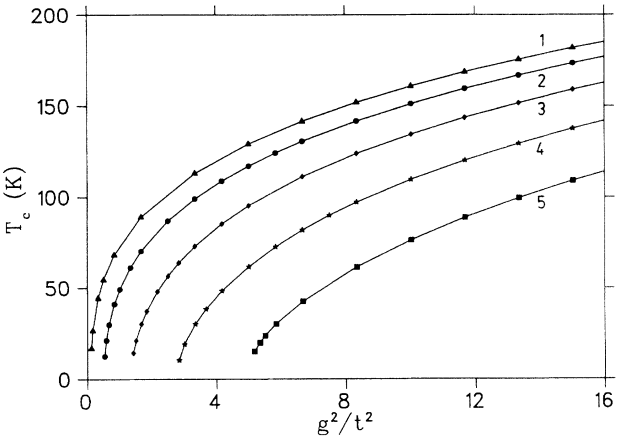

FIG. 8. The calculations of T_c from Eqs. (35) and (36) for different g and μ with the spectral function given by Eq. (42). The value of t is 100 meV, $\omega_0 = 0.08t$, and $\omega_{\max} = 4t$. Curve (1) is for $\mu = -0.1t$, curve (2) is for $\mu = -0.2t$, curve (3) is for $\mu = -0.3t$, curve (4) is for $\mu = -0.4t$, and curve (5) is for $\mu = -0.5t$.

The results of a numerical solution of Eqs. (35) and (36) for the critical temperature are shown in Fig. 8 for different values of g and μ. The numerical procedure used to calculate T_c is the same as in the preceding subsection and is based on finding the highest temperature at which the maximum eigenvalue of the kernel in the symmetrized form of Eq. (36) is one[3] (for details see Ref. 28). The spectral function $P(\Omega)$ is taken to have the following form:

$$P(\Omega) = \left[\frac{\Omega}{\omega_0^2}\theta(\omega_0-\Omega) + \frac{1}{\Omega}\theta(\Omega-\omega_0)\theta(\omega_{\max}-\Omega)\right]\left[\ln\frac{\omega_{\max}}{\omega_0} + \frac{1}{2}\right]. \tag{42}$$

Thus, $P(\Omega)$ increases linearly for $0 \le \Omega \le \omega_0$ and decreases as $1/\Omega$ for $\omega_0 \le \Omega \le \omega_{\max}$. The cutoff in the sums over Matsubara frequencies is $5\omega_{\max}$. In this subsection all energy variables are in units of t, where $8t$ is the bandwidth. We take $t = 100\,\text{meV}$. The interesting feature of the dependence of T_c on g and μ is the existence of lower thresholds for the values of g at each given μ, as predicted by the square-well model. However, while at large g the square-well model predicts a linear increase of T_c with g^2 [see Eq. (38)], the rate of increase in T_c obtained from numerical solutions of self-consistent Eqs. (35) and (36) decreases with increasing g^2.

After including the second-order graph, the T_c equations take the form:

$$Z_n(\mathbf{k}) = 1 + \frac{\pi T}{|\omega_n|}\sum_{n'}\lambda_s(n-n')A_{nn'}(\mathbf{k},\mathbf{k}+\mathbf{Q})G_{n'}(\mathbf{k}+\mathbf{Q})s_n s_{n'}\,, \tag{43}$$

$$Z_n(\mathbf{k})\Delta_n(\mathbf{k}) = -\pi T\sum_{n'}\left[\lambda_s(n-n')B_{nn'}(\mathbf{k},\mathbf{k}+\mathbf{Q})G_{n'}(\mathbf{k}+\mathbf{Q})\frac{\Delta_{n'}(\mathbf{k}+\mathbf{Q})}{|\omega_{n'}|}\right.$$
$$\left. + C_{nn'}(\mathbf{k},\mathbf{k})G_{n'}(\mathbf{k})\frac{\Delta_{n'}(\mathbf{k})}{|\omega_{n'}|}\right], \tag{44}$$

where

$$A_{nn'}(\mathbf{k},\mathbf{k}+\mathbf{Q}) = 1 - \alpha_s \pi T \sum_{n''} \lambda_s(n'') G_{n+n''}(\mathbf{k}+\mathbf{Q}) G_{n'+n''}(\mathbf{k}) \times \left(s_{n+n''} s_{n'+n''} - \tilde{\epsilon}_{n+n''}(\mathbf{k}+\mathbf{Q}) \frac{2\tilde{\epsilon}_{n'+n''}(\mathbf{k}) + \tilde{\epsilon}_{n'}(\mathbf{k}+\mathbf{Q})\omega_{n'+n''}/\omega_{n'}}{|\omega_{n+n''}\omega_{n'+n''}|} \right) , \quad (45)$$

$$B_{nn'}(\mathbf{k},\mathbf{k}+\mathbf{Q}) = 1 - \alpha_s 2\pi T \sum_{n''} \lambda_s(n'') G_{n+n''}(\mathbf{k}+\mathbf{Q}) G_{n'+n''}(\mathbf{k}) \times \left(s_{n+n''} s_{n'+n''} - \frac{\tilde{\epsilon}_{n+n''}(\mathbf{k}+\mathbf{Q})\tilde{\epsilon}_{n'+n''}(\mathbf{k})}{|\omega_{n+n''}\omega_{n'+n''}|} \right) , \quad (46)$$

$$C_{nn'}(\mathbf{k},\mathbf{k}) = \alpha_s \pi T \sum_{n''} \lambda_s(n-n'') \lambda_s(n'-n'') G_{n''}(\mathbf{k}+\mathbf{Q}) G_{n+n'-n''}(\mathbf{k}+\mathbf{Q}) \times \left(s_{n''} s_{n+n'-n''} - \frac{\tilde{\epsilon}_{n''}(\mathbf{k}+\mathbf{Q})\tilde{\epsilon}_{n+n'-n''}(\mathbf{k}+\mathbf{Q})}{|\omega_{n''}\omega_{n+n'-n''}|} \right) . \quad (47)$$

By comparing Eqs. (35) and (36) with Eqs. (43) and (44), one sees that to include the second-order graph in the T_c equations one has to multiply $\lambda_s(n-n')$ in Eqs. (35) and (36) by the matrices $A_{nn'}(\mathbf{k},\mathbf{k}+\mathbf{Q})$ and $B_{nn'}(\mathbf{k},\mathbf{k}+\mathbf{Q})$, respectively, and add the additional term with matrix $C_{nn'}(\mathbf{k},\mathbf{k})$ in Eq. (36). The results of the numerical calculations are shown in Fig. 9. The effect of the second-order graph on T_c is much more pronounced than in the isotropic case. Moreover, the T_c is very sensitive to μ and for certain values of μ the second-order graph leads to an increase of T_c, in contrast to the isotropic case. For $\mu = -0.2t$ the T_c is increased by about 50%. However, for larger absolute values of μ the suppression of T_c by the lowest-order vertex correction can be very large. It should be noted that the dependence on μ at $\alpha_s = 1/3$ (which corresponds to the full value of the second-order graph) is nonmonotonic. The absolute changes in T_c calculated from Eqs. (42)–(46) compared to $T_c^{(1)} = 100$ K calculated from the first-order self-energy graph are shown in Fig. 10. We would like to emphasize that at a fixed $T_c^{(1)}$ (and consequently different values of g for different values of μ) the relative changes in T_c are quite similar to those obtained for fixed g (and consequently different values of $T_c^{(1)}$ for different values of μ).

In order to understand the qualitative difference between this model and the isotropic case, one has to examine the relative size and the sign of the changes in T_c arising from the correction terms in the matrices A, B, and C, taken separately. To this end one can use instead of α_s three independent prefactors α_s^A, α_s^B, and α_s^C in Eqs. (45)–(47), respectively. One finds that both $A_{nn'}(\mathbf{k},\mathbf{k}+\mathbf{Q})$ and $C_{nn'}(\mathbf{k},\mathbf{k})$ lead to an increase of T_c, while $B_{nn'}(\mathbf{k},\mathbf{k}+\mathbf{Q})$ produces a decrease of T_c. The important difference between this model and the isotropic

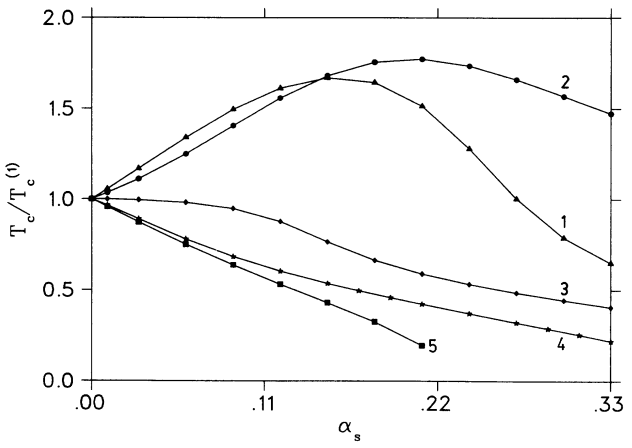

FIG. 9. The relative changes of T_c as a function of a parameter α_s, which controls the size of the contribution from the second-order graph, compared to $T_c^{(1)}$ calculated from the first-order graph. The parameters t, ω_0, and ω_{max} are the same as in Fig. 8. The interaction constant g is equal to $2.95t$. Curve (1) is for $\mu = -0.1t$, curve (2) is for $\mu = -0.2t$, curve (3) is for $\mu = -0.3t$, curve (4) is for $\mu = -0.4t$, and curve (5) is for $\mu = -0.5t$.

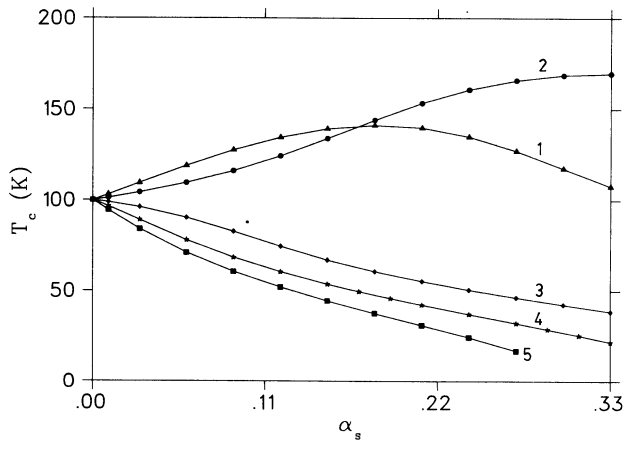

FIG. 10. The absolute changes in T_c as a function of a parameter α_s at fixed $T_c^{(1)} = 100$ K. Curve (1) is for $\mu = -0.1t$, $g = 1.52t$, curve (2) is for $\mu = -0.2t$, $g = 1.85t$, curve (3) is for $\mu = -0.3t$, $g = 2.33t$, curve (4) is for $\mu = -0.4t$, $g = 2.95t$, and curve (5) is for $\mu = -0.5t$, $g = 3.67t$.

case is the change in sign of the effect of the C matrix. In both the isotropic case and the model with four sharp peaks in magnetic susceptibility the effect of the correction term in matrix A is to enhance T_c, since it reduces the renormalization function Z. Also, the effect of the correction term in matrix B, which is always larger than the effects of either the correction term in A or C taken separately, is to suppress T_c in both cases. However, due to the symmetry of the gap function given by Eq. (39) for the model with four sharp peaks, the effect of the matrix C, which results from the crossed-line diagram with the anomalous Green's function as the middle line [see the second line in Fig. 7(b)], is to increase the T_c. This is because $\Delta_n(\mathbf{k})$ and $\Delta_n(\mathbf{k}+\mathbf{Q})$ have different signs [see Eq. (44)]. In the isotropic case, however, this effect is absent, and the matrix C has the same effect on T_c as the correction term in matrix B—it reduces the T_c. For certain not too large values of μ, the combined effect of matrices A and C can be larger than the effect produced by the matrix B, which results in enhancement of T_c by the second-order graph. However, as is clear from Fig. 10, the dependence on μ for the full value of the correction from the second-order graph (i.e., for $\alpha_s = 1/3$) is nonmonotonic, and no simple dependence of this correction on μ could be found. This is in contrast to the T_c calculated from the first-order graph, Eqs. (35)–(37), where for a fixed g and $P(\Omega)$ the T_c decreases with increasing μ (see Fig. 8).

IV. CONCLUSIONS

In summary, we have found that including the vertex corrections in the calculations of T_c for the BCS-type interaction leads to a decrease of T_c. This result is general as long as the BCS interaction parameter λ is less than 1. Beyond a certain critical value of ω_c/E_F, which decreases with increasing λ, there is no finite solution to the T_c equation, regardless of the dimensionality of the system. This is a new result which, together with our numerical calculations, gives more quantitative information about the limits of validity of the BCS pairing model than known previously.[1]

The self-consistent calculations of the strong-coupling equations generalized to include the contribution from the diagram with two crossed boson lines for an isotropic pairing interaction give results, which are completely analogous to the BCS case. The main difference between the BCS case and the theory that takes into account the time dependence of the interaction is that in the latter case a reduction in the renormalization function due to the second-order graph slows down the decrease in T_c with increasing ω_c/E_F. Our numerical calculations show that for the values of the maximum phonon energy and the Fermi energy that are typical for simple metals the corrections from the lowest-order vertex correction are in the limits estimated by Eliashberg's[19] generalization of the Migdal's theorem[18] to the superconducting state. However, if $\omega_c/E_F = O(1)$, as has been suggested for doped fullerenes,[2] the vertex corrections could not be ignored, nor is it sufficient to stop at the lowest-order vertex correction, unless λ is small, since the correct expansion parameter in the theory is $\lambda(\omega_c/E_F)$. When this parameter is not smaller than 1 it is unreasonable to expect that somehow all the vertex corrections cancel, so that one could still use various approximate T_c formulas[3] which are based on the one-boson exchange graph.

For a highly anisotropic interaction of the type used in the antiferromagnetic spin-fluctuation theories of superconductivity in copper oxides, the corrections could be qualitatively and quantitatively different. For a model spin susceptibility with four sharp peaks in the corners of a square Brillouin zone we find a substantial increase of T_c due to the second-order graph for certain values of the chemical potential μ, which is related to the amount of doping away from the half filling. The key reason for this reversal of sign of the correction to the T_c compared to the isotropic case is the symmetry of the gap function

$$\Delta_n(\mathbf{k}) = \Delta_n^{\alpha}(\mathbf{k})[\cos(k_x a) + \alpha\cos(k_y a)],$$

where $\alpha = \pm 1$. This form of the gap function implies that the diagrams in the second row in Fig. 7(b) for the pairing self-energy reverse the sign compared to the isotropic case. However, for large enough μ, the remaining diagrams give a larger negative contribution to the pairing self-energy, with a net result similar to what is found in the isotropic case. We note that the sign of the correction to the T_c from the second order graph is a nonmonotonic function of μ, and the maximum T_c is obtained for $\mu = -0.2t$ (see Fig. 10). The changes in T_c (either an increase or a decrease) caused by the second-order graph in this model can be large enough to render a result obtained from the one-boson exchange graph highly inaccurate.

ACKNOWLEDGMENTS

The authors are thankful to J. P. Carbotte and A-M. S. Tremblay for stimulating discussions. This work was supported by the Natural Sciences and Engineering Research Council of Canada.

APPENDIX A: FUNCTION $\kappa(T)$

In this appendix we summarize the analytical calculations of the correction term [see Eqs. (7) and (8)] to the BCS equation for the critical temperature. Since $\Delta_p = \Delta\theta(\omega_c - |\epsilon_p|)$ (see Sec. II), the order parameter drops out of Eq. (7), and one finds that the usual T_c equation is corrected by the term

$$\delta V(T) = -VT^2 \sum_{n',n''} \sum_{\mathbf{p}',\mathbf{p}''} \frac{\delta V_{p',p''}^{n',n''}}{(\omega_{n'}^2 + \epsilon_{p'}^2)(\omega_{n''}^2 + \epsilon_{p''}^2)} . \quad \text{(A1)}$$

The dependence on momenta is through the energies and after the transformation of the momentum sums to the integrals over the energy variables one can write Eq. (A1) as

$$\delta V(T) = -\lambda^3 \frac{T^2}{8E_F} \sum_{n'n''} \int_{-\omega_c}^{\omega_c} d\epsilon_1 \int_{-\omega_c}^{\omega_c} d\epsilon_2 \int_{-\omega_c}^{\omega_c} d\epsilon_3 \int_{-\omega_c}^{\omega_c} d\epsilon_4 \times \frac{1}{(\omega_{n'}^2 + \epsilon_1^2)} \frac{1}{(\omega_{n''}^2 + \epsilon_2^2)} \frac{\tanh(\epsilon_3/2T) - \tanh(\epsilon_4/2T)}{i\nu_{n'+n''} + \epsilon_3 - \epsilon_4} M(p_1, p_3; p_2, p_4) \,. \tag{A2}$$

Here, $p_i = \sqrt{2m(E_F - \epsilon_i)}$ $(i = 1, 2, 3, 4)$. The function $M(p_1, p_3; p_2, p_4)$ is determined by the dimensionality of the system

$$M(p_1, p_3; p_2, p_4) = \int_{Q_m}^{Q_M} \frac{dQ}{2p_F} \times \begin{cases} 1 & \text{in 3D} \\ 4p_F^3 \pi^{-2} Q X(Q, p_1, p_3)^{-1} X(Q, p_2, p_4)^{-1} & \text{in 2D} \,, \end{cases} \tag{A3}$$

where $p_F = \sqrt{2mE_F}$, $X(Q, p, p') = \sqrt{Q^2 - (p - p')^2}\sqrt{(p + p')^2 - Q^2}$, $Q_M = \min(p_1 + p_3, p_2 + p_4)$, and $Q_m = \max(|p_1 - p_3|, |p_2 - p_4|)$. Since all the energies–and thus the corresponding momenta—are restricted to the energy shell of the half width ω_c, one can expand in ω_c/E_F. In 3D, the result is

$$M(p_1, p_3; p_2, p_4) = 1 + O\left(\frac{\omega_c}{E_F}\right) \tag{A4}$$

and in 2D,

$$M(p_1, p_3; p_2, p_4) = \pi^{-2} \left[\ln \frac{8E_F}{|\epsilon_1 + \epsilon_2 - \epsilon_3 - \epsilon_4|} + \ln \frac{8E_F}{|\epsilon_1 - \epsilon_2 + \epsilon_3 - \epsilon_4|} + \ln \frac{8E_F}{|\epsilon_1 - \epsilon_2 - \epsilon_3 + \epsilon_4|} \right] + O\left(\frac{\omega_c}{E_F}\right) . \tag{A5}$$

It is sufficient to consider only the three-dimensional case, since the two-dimensional result can be obtained with a sufficient accuracy from the one in 3D by using for M a constant $\simeq (3/\pi^2)\ln(8E_F/\omega_c)$ instead of 1. Thus, the expression for $\delta V(T)$ takes the form

$$\delta V(T) = -\lambda^3 \frac{\pi^2 T^2}{2E_F} \sum_{n', n''} \frac{a_{n'}}{|\omega_{n'}|} \frac{a_{n''}}{|\omega_{n''}|} \int_0^{\omega_c} d\epsilon \tanh \frac{\epsilon}{2T} \ln \frac{(\omega_c + \epsilon)^2 + \nu_{n'+n''}^2}{(\omega_c - \epsilon)^2 + \nu_{n'+n''}^2} \,, \tag{A6}$$

where $a_n = (2/\pi)\arctan(\omega_c/|\omega_n|)$. At $T \ll \omega_c$ the integral in Eq. (A6) is equal to $(4\ln 2)\omega_c$. The BCS integral from Eq. (10) can be written in the following form:

$$\Lambda(T) = \pi\lambda T \sum_n \frac{a_n}{|\omega_n|} \,. \tag{A7}$$

It is convenient to introduce a function $\kappa(T)$

$$\kappa(T) = -\frac{\delta V(T) E_F}{\lambda \omega_c \Lambda(T)^2} , \tag{A8}$$

which is a universal function of $\omega_c/\pi T$ and has to be calculated numerically. One finds $\kappa(T) = O(1)$ and it can be proven analytically that $\kappa(T) \to \ln 4$ when $T \to 0$ (see Fig.2). After expressing $\delta V(T)$ in terms of $\kappa(T)$ one immediately arrives at Eq. (9).

APPENDIX B: CORRECTIONSTO ISOTROPIC ELIASHBERG EQUATIONS IN 2D

In this appendix we derive the matrices $A(n, n')$, $B(n, n')$, and $C(n, n')$ in 2D. The starting equation is Eq. (21) for $\hat{\Sigma}^{(2)}$. After making the approximation (24) for $M(k, k'''; k', k'')$, one has to evaluate the integrals over the energy variables. Because of the prefactor E_F^{-1} in the expression for $\hat{\Sigma}^{(2)}$ these integrals can be evaluated with the accuracy $O(\omega_c/E_F)$. For ϵ_p and $|\omega_i| \lesssim \omega_c$ one has

$$\int_{-E_F}^{E_F}\frac{|\omega_1|d\epsilon_1}{\omega_1^2+\epsilon_1^2}\int_{-E_F}^{E_F}\frac{|\omega_2|d\epsilon_2}{\omega_2^2+\epsilon_2^2}\int_{-E_F}^{E_F}\frac{|\omega_3|d\epsilon_3}{\omega_3^2+\epsilon_3^2}\ln|\epsilon_1+\epsilon_2+\epsilon_3+\epsilon_p|$$

$$=\frac{\pi^3}{2}\ln\left[(|\omega_1|+|\omega_2|+|\omega_3|)^2+\epsilon_p^2\right]a_1a_2a_3+O(\omega_c/E_F),$$

$$\int_{-E_F}^{E_F}\frac{|\omega_1|d\epsilon_1}{\omega_1^2+\epsilon_1^2}\int_{-E_F}^{E_F}\frac{\epsilon_2 d\epsilon_2}{\omega_2^2+\epsilon_2^2}\int_{-E_F}^{E_F}\frac{\epsilon_3 d\epsilon_3}{\omega_3^2+\epsilon_3^2}\ln|\epsilon_1+\epsilon_2+\epsilon_3+\epsilon_p|=-\frac{7\pi}{2}\zeta(3)a_1+O(\omega_c/E_F), \tag{B1}$$

where ζ is the usual Riemann zeta function. The factors $a_i=(2/\pi)\arctan(E_F/|\omega_i|)$ are kept for convenience, since they provide an additional cutoff at high Matsubara frequencies. By using Eq. (B1) one finds

$$A(n,n';\epsilon_p)=1-\frac{3T}{E_F}\sum_{n''}\lambda(n-n'')\left[s_{n'+n''-n}s_{n''}a_{n'+n''-n}a_{n''}\right.$$
$$\left.\times\ln\frac{8E_F}{\sqrt{\epsilon_p^2+(|\omega_{n'}|+|\omega_{n'+n''-n}|+|\omega_{n''}|)^2}}+\frac{7\zeta(3)}{3\pi^2}(1-\tfrac{1}{2}s_{n'}s_{n'+n''-n}a_{n'+n''-n}/a_{n'})\right],$$

$$B(n,n';\epsilon_p)=1-\frac{6T}{E_F}\sum_{n''}\lambda(n-n'')\left[s_{n'+n''-n}s_{n''}a_{n'+n''-n}a_{n''}\right.$$
$$\left.\times\ln\frac{8E_F}{\sqrt{\epsilon_p^2+(|\omega_{n'}|+|\omega_{n'+n''-n}|+|\omega_{n''}|)^2}}+\frac{7\zeta(3)}{6\pi^2}\right],$$

$$C(n,n';\epsilon_p)=\frac{3T}{E_F}\sum_{n''}\lambda(n-n'')\lambda(n''-n')\left[s_{n'+n''-n}s_{n''}a_{n'+n''-n}a_{n''}\right.$$
$$\left.\times\ln\frac{8E_F}{\sqrt{\epsilon_p^2+(|\omega_{n'}|+|\omega_{n'+n''-n}|+|\omega_{n''}|)^2}}-\frac{7\zeta(3)}{6\pi^2}\right]. \tag{B2}$$

---

* Present address: Department of Physics, University of Maryland, College Park, Maryland 20742-4111.

[1] A. A. Abrikosov, L. P. Gor'kov, and I. Ye. Dzyaloshinsky, *Quantum Field Theoretical Methods in Statistical Physics* (Pergamon, New York, 1965).

[2] I. I. Mazin, S. N. Rashkeev, V. P. Antropov, O. Jepsen, A. I. Liechtenstein, and O. K. Andersen, Phys. Rev. B **45**, 5114 (1992); V. P. Antropov, O. Gunarsson, and A. I. Liechtenstein, *ibid.* **48**, 7651 (1993).

[3] P. B. Allen and B. Mitrović, in *Solid State Physics*, edited by H. Ehrenreich, F. Seitz, and D. Turnbull (Academic, New York, 1992), Vol. 37, p. 1.

[4] D. J. Scalapino, in *Superconductivity*, edited by R. D. Parks (Dekker, New York, 1969), Vol. 1, p. 449.

[5] H. Rietschel and L. J. Sham, Phys. Rev. B **28**, 5100 (1983).

[6] M. Grabowski and L. J. Sham, Phys. Rev. B **29**, 6132 (1984).

[7] H. R. Krishnamurthy, D. M. Newns, P. C. Pattnaik, C. C. Tsuei, and C.C. Chi, Phys. Rev. B **49**, 3520 (1994).

[8] P. Monthoux and D. Pines, Phys. Rev. Lett. **69**, 961 (1992); Phys. Rev. B **47**, 6069 (1993).

[9] R. J. Radtke, K. Levin, H.-B. Schüttler, and M. R. Norman, Phys. Rev. B **48**, 15 957 (1993).

[10] S. Lenck and J. P. Carbotte, Phys. Rev. B **46**, 14 850 (1992).

[11] P. Monthoux, A. V. Balatsky, and D. Pines, Phys. Rev. B **46**, 14 803 (1992).

[12] P. Monthoux and D. J. Scalapino, Phys. Rev. Lett. **72**, 1874 (1994).

[13] S. Lenck, J. P. Carbotte, and R. C. Dynes, Phys. Rev. B **49**, 9111 (1994).

[14] N. Bulut, D. J. Scalapino, and S. R. White, Phys. Rev. B **47**, 2742 (1993); **47**, 6157 (1993).

[15] The order of the magnitude of $\delta V_{p,p'}^{n,n'}$ is $\lambda^2\omega_c^2/E_F$, and it has an additional smallness due to the parameter ω_c/E_F. The diagram with three crossed interaction lines has the order of $\lambda^3\omega_c^3/E_F^2$ in three dimensional case and $\lambda^3\omega_c^2/E_F$ in two dimensional case. For details, see V. N. Kostur and B. Mitrović, Phys. Rev. B **48**, 16 388 (1993).

[16] J. R. Schrieffer, *Theory of Superconductivity* (Benjamin, New York, 1964).

[17] J. R. Schrieffer, J. Appl. Phys. **39**, 646 (1968).

[18] A. B. Migdal, Zh. Eksp. Teor. Fiz. **34**, 1438 (1958) [Sov. Phys. JETP **7**, 996 (1958)].

[19] G. M. Eliashberg, Zh. Eksp. Teor. Fiz. **38**, 966 (1960) [Sov. Phys. JETP **11**, 696 (1960)].

[20] G. M. Eliashberg, in *High Temperature Superconductivity from Russia*, edited by A. I. Larkin and N. V. Zavaritsky (World Scientific, Singapore, 1989); see also V. N. Kostur and B. Mitrović, in Ref. 15.

[21] J. A. Hertz, K. Levin, and M. T. Beal-Monod, Solid State Commun. **18**, 803 (1976); B. Mitrović and J. P. Longo, *ibid.* **67**, 935 (1988).
[22] For details, see V. N. Kostur and B. Mitrović, in Ref. 15.
[23] J. M. Rowell, W. L. McMillan, and R. C. Dynes (unpublished).
[24] N. W. Ashkroft and N. D. Mermin, *Solid State Physics* (Holt, Rinehart and Winston, New York, 1976).
[25] A. P. Kampf and J. R. Schrieffer, Phys. Rev. B **41**, 6399 (1990); **42**, 7967 (1990).
[26] A. Millis, H. Monien, and D. Pines, Phys. Rev. B **42**, 167 (1990).
[27] The limit $\Gamma \to \infty, \chi_\Gamma/\Gamma^2 = \text{const}$ in Eq. (34) gives the spin susceptibility in the isotropic case. In the case of four δ peaks in the corners of the Brillouin zone one finds that the derivatives of the self-energy $\Sigma(\omega, \epsilon_{\mathbf{k}})$ with respect to ω and $\epsilon_{\mathbf{k}}$ have the same order of magnitude: $\partial\Sigma(\omega, \epsilon_{\mathbf{k}})/\partial\epsilon_{\mathbf{k}} \sim \partial\Sigma(\omega, \epsilon_{\mathbf{k}})/\partial\omega$. Also at $T = 0$ $\mathrm{Im}\Sigma(\omega, \epsilon_{\mathbf{k}}) \propto P(\omega)$ at small ω, while in the isotropic case $\mathrm{Im}\Sigma(\omega, \epsilon_{\mathbf{k}}) \propto \int_0^\omega d\Omega P(\Omega)$.
[28] V. N. Kostur and B. Mitrović (unpublished).
[29] Usually the square-well model implies different approximations for $\lambda(n - n')$ in the renormalization and the pairing channel (see Ref. 3). However, in order to obtain the analytical results we have to take the BCS limit, which amounts to using the same approximation in both channels, so that $Z_n(\mathbf{k}) = 1$.